

DL-Polycube: Deep learning enhanced polycube method for high-quality hexahedral mesh generation and volumetric spline construction

Yuxuan Yu^{1*}, Yuzhuo Fang¹, Hua Tong², Yongjie Jessica Zhang^{2*}

^{1*}Institute of Artificial Intelligence, Donghua University, 2999 North Renmin Road, Shanghai, 201620, China

²Department of Mechanical Engineering, Carnegie Mellon University, 5000 Forbes Ave, Pittsburgh, 15213, PA, USA

*Corresponding author(s). E-mail(s): yuyuxuan@dhu.edu.cn;
jessicaz@andrew.cmu.edu;

Contributing authors: slccovey@outlook.com; huat2@andrew.cmu.edu;

Abstract

In this paper, we present a novel algorithm that integrates deep learning with the polycube method (DL-Polycube) to generate high-quality hexahedral (hex) meshes, which are then used to construct volumetric splines for isogeometric analysis. Our DL-Polycube algorithm begins by establishing a connection between surface triangular meshes and polycube structures. We employ deep neural network to classify surface triangular meshes into their corresponding polycube structures. Following this, we combine the acquired polycube structural information with unsupervised learning to perform surface segmentation of triangular meshes. This step addresses the issue of segmentation not corresponding to a polycube while reducing manual intervention. Quality hex meshes are then generated from the polycube structures, with employing octree subdivision, parametric mapping and quality improvement techniques. The incorporation of deep learning for creating polycube structures, combined with unsupervised learning for segmentation of surface triangular meshes, substantially accelerates hex mesh generation. Finally, truncated hierarchical B-splines are constructed on the generated hex meshes. We extract trivariate Bézier elements from these splines and apply them directly in isogeometric analysis. We offer several examples to demonstrate the robustness of our DL-Polycube algorithm.

Keywords: polycube, graph convolutional network, hexahedral mesh generation, volumetric spline construction, isogeometric analysis

1 Introduction

Isogeometric analysis (IGA) is an analysis method designed to unify finite element analysis (FEA) and computer-aided design (CAD) by using the same basis functions for both geometrical and simulation representation [1]. Introduced by T.J.R. Hughes in 2005 [2], IGA has evolved significantly over the past two decades. Despite these advancements, constructing volumetric parameterization from surfaces remains a challenging task. Most CAD software represents geometry using boundary representation (B-Rep) models, typically expressed mathematically through NURBS (Non-Uniform Rational B-Splines). These B-Rep models are composed of multiple B-spline or NURBS patches. Consequently, IGA initially focused on B-Rep models [2]. In 2003, T.W. Sederberg introduced T-splines [3], which allow for T-junctions in quadrilateral control meshes, enabling local refinement. However, traditional T-splines lack linear independence and partition of unity properties, making them unsuitable for IGA and design. Recent research has developed analysis-suitable T-splines for IGA [4], particularly for shell structures [5]. Although B-Rep model parameterization is often used in IGA, three-dimensional (3D) solid models often have advantages over B-Rep models which discard internal geometric information. IGA often requires volumetric representation to account for internal material structures and densities. Therefore, constructing volumetric spline parameterization models suitable for IGA has been a persistent challenge in applying IGA to 3D solid models.

Research on constructing volumetric parameterization for IGA can be categorized into two main approaches based on the input: constructive solid geometry (CSG) [6] and B-Rep [7, 8]. However, CSG-based models pose difficulties for IGA due to the presence of trimming surfaces. B-Rep models require generating control meshes and constructing volumetric spline basis functions. In FEA, B-Rep models can be discretized into tetrahedral or hexahedral (hex) meshes. While tetrahedral mesh generation has multiple automatic strategies and is widely used in industry, hex meshes are preferred for their advantages: fewer elements for the same accuracy [9], avoidance of tetrahedral locking [10], and better suitability for tensor-product spline construction.

Despite ongoing research in hex mesh generation [11–13], generating high-quality hex meshes for complex B-Rep models remains challenging. Methods like indirect methods [14], sweeping methods [15, 16], grid-based methods [17–19], polycube methods [20–24], and vector field-based methods [25, 26] have been explored. However, not all these methods are suitable for IGA. Hex meshes often involve extraordinary points (an extraordinary point has other than four faces adjacent to it) or extraordinary edges (an extraordinary edge is an interior edge shared by other than four hex elements), which can complicate spline construction and parameterization. When extraordinary points or extraordinary edges are involved, achieving optimal convergence rates is a challenging problem in IGA, even smooth basis functions are defined around them. To minimize the number of extraordinary points and extraordinary edges, sweeping and polycube methods are preferred for generating hex control meshes for IGA. Sweeping methods produce high-quality meshes by scanning from source to target surfaces, but their applicability is limited to specific models where the source and target surfaces have similar topology. Polycube methods use polycubes as parameter spaces to generate hex meshes through parametric mapping. The concept of polycubes was first

introduced as a texture mapping technique for general meshes [20]. Lin *et al.* [27] proposed an automated method for constructing polycubes; however, this method is not suitable for models with complex topology and geometry. Due to the polycube method’s capability of controlling the location of extraordinary points and edges, and because the polycube structure and parametric mapping can be used together to generate 3D T-spline models [8], the polycube method has been employed to generate hex control meshes. Hu *et al.* [23, 28] used centroidal Voronoi tessellation to segment surfaces and generated hex control meshes using the polycube method. Guo *et al.* [29] introduced extraordinary edges within the polycube to improve mesh quality. Li *et al.* [30] proposed the generalized polycube method, significantly improving the adaptability of the polycube method to high-genus B-Rep models. Yu *et al.* [24] used CVT to segment surfaces and generated generalized polycubes with internal extraordinary edges, subsequently generating hex control meshes through the generalized polycube method.

Constructing splines on hex control meshes is another challenge. Various spline techniques like NURBS [15], T-splines [8, 21, 22], and TH-splines [31] have been developed for volumetric parameterization. It involves achieving optimal convergence rates and minimizing geometric errors. Optimal convergence rates are related to the extraordinary points and edges of the control mesh. For geometric errors, global or local refinement combined with spline fitting can be employed. Compared to globally subdividing the entire space, local refinement can accurately fit surface geometry using fewer control points. Xu *et al.* [32] optimized the positions of control points in regions with significant geometric features and errors through r-adaptive framework. Li *et al.* [30] used the local refinement capability of T-splines to reduce geometric errors when fitting surface models. However, for B-Rep models with complex surface features, regions with significant geometric errors usually occur around the geometric features. If the control mesh does not preserve these features, it can indirectly affect the magnitude of geometric errors. Therefore, when global or local refinement cannot significantly reduce geometric errors, further processing of the control mesh is necessary, which includes adding feature information to the hex control mesh.

To address these challenges, we developed HexGen and Hex2Spline [24] in our previous research. HexGen generates hex meshes, while Hex2Spline uses them as the input control meshes to construct volumetric truncated hierarchical splines. Through Bézier extraction, Hex2Spline transfers spline information to ANSYS-DYNA for IGA. Our results demonstrate the algorithm’s capability to generate analysis-suitable volumetric parameterization models for IGA. However, the process involves significant manual work in the input file preparation, which includes surface segmentation and polycube construction. The automation of surface segmentation and polycube construction was also discussed in a 2023 survey paper [11], where it was defined as labeling. In this context, the polycube structure can be defined by assigning a label to each surface triangular element of the input mesh. Early labeling methods used the six principal axes ($\pm X$, $\pm Y$, $\pm Z$). The first issue is that this approach is suitable for models where any face is roughly perpendicular to one of the six normal directions. However, forcing a regular structured polycube to fit some complex geometries results in poor quality meshes. Another issue is that different approaches produce different labelings, such

as the centroidal Voronoi tessellation method [23], local approaches [33], and incremental approaches [34]. In addition, not all labelings result in a valid polycube. Some researchers [33, 35, 36] have proposed adjustment methods, but these methods are neither robust nor straightforward [11].

In this paper, we focus on replacing the manual surface segmentation process and polycube construction with intelligent, automated methods. To reduce manual labor, we integrate deep learning into the polycube method, developing the deep learning-enhanced polycube (DL-Polycube) algorithm. This method predicts the polycube structure of input geometries and segments geometry surfaces to match the polycube structure, automating the surface segmentation and polycube construction process. The DL-Polycube algorithm significantly enhances the efficiency of our previously developed HexGen and Hex2Spline software packages by minimizing the manual effort required for surface segmentation and polycube construction. In summary, there are three main contributions in this paper.

1. Unlike the traditional sequence of generating hex meshes based on polycubes, the DL-Polycube algorithm employs machine learning to automatically construct polycube structures from input geometries and then perform surface segmentation based on these polycube structures. This approach aligns more closely with domain knowledge or human intuition. A skilled mesh generation engineer typically spends time optimally deciding how to partition complex geometries into simpler regions before manually generating hex meshes. They then create quadrilateral surface meshes on each partitioned block and use mapping or sweeping methods to generate hex meshes within the volumes. Our method approximates this process using machine learning.
2. The DL-Polycube algorithm demonstrates its capability in rapidly predicting the corresponding polycube structure of geometric models and segmenting the surface of CAD geometry to achieve a one-to-one correspondence with the surface of the polycube structure. By integrating deep learning with the polycube method, we automate the process of converting CAD geometries into high-quality hex meshes and volumetric spline models. The entire prediction step completes in one second for a single model. Our approach demonstrates that machine learning can effectively automate and optimize the mesh generation process.
3. The DL-Polycube algorithm enhances the efficiency of our previously developed HexGen and Hex2Spline software packages. Although these packages can handle complex models, they require suitable input files, which involve manual work for surface segmentation and polycube structure construction. By integrating deep learning, we reduce this manual effort by replacing the manual surface segmentation process and polycube construction with intelligent, automated methods. This significantly reduces the learning curve for the software.

The remainder of this paper is organized as follows. Section 2 provides an overview of the pipeline, including the design of the DL-Polycube algorithm. Section 3 details the implementation of the DL-polycube method, including dataset generation and curation, and the machine learning model. Section 4 discusses machine learning-driven polycube-based segmentation and path optimization for zigzag issues. Section 5 covers high-quality hex mesh generation and volumetric spline construction. Section 6

presents examples to demonstrate the feasibility and efficiency of the algorithm in generating hex meshes and splines. Finally, Section 7 concludes and suggests future work.

2 Overview of the pipeline

2.1 Pipeline design

We integrate deep learning with the polycube method to convert CAD geometries into volumetric spline models. As shown in Fig. 1, our DL-Polycube pipeline begins with the conversion of the CAD geometry into a triangular mesh. Subsequently, a pretrained deep learning model is used to generate a polycube structure. This structure serves as the foundation for generating all-hex meshes through parametric mapping [37] and octree subdivision techniques [8]. To ensure the all-hex mesh meets the quality requirements necessary for IGA, we evaluate the all-hex mesh and employ several mesh quality improvement techniques—pillowing [38], smoothing, and optimization [17, 39]—as needed. Upon achieving a good quality hex mesh, the volumetric spline model is constructed from the hex mesh using TH-spline3D with local refinement. Then the Bézier information is extracted to perform IGA in ANSYS-DYNA.

2.2 DL-Polycube algorithm

The DL-Polycube algorithm includes three steps, which are training dataset generation and curation, graph convolutional network polycube (GCN-polycube) recognition, and K-means surface segmentation (see Fig. 2). This DL-Polycube method leverages the efficiency of machine learning to handle a wide range of CAD geometries, replacing the manual surface segmentation and polycube construction [22] with intelligent, automated methods. The success of this algorithm is based on the following assumption: *although there are inconsistencies in the geometry models, the underlying polycube structure may remain topologically consistent*. By utilizing a pretrained machine learning model, the algorithm can identify the most suitable polycube for unfamiliar geometries, thereby automating and optimizing the process. Consequently, this leads to a powerful tool for generating high-quality hex meshes and constructing volumetric splines from CAD geometry.

In the dataset generation and curation step, we create a corresponding cage around the target mesh that requires deformation (e.g., a cube). The deformation of the cage influences the inner mesh. Deformations are performed by randomly selecting points on the cage, stretching them to lengths that follow a normal distribution. The entire process is conducted in Blender, a free and open-source 3D creation suite, producing effects similar to classical free-form deformation [40, 41]. This method enables the generation of a diverse set of models with random transformations and deformations.

In the GCN-Polycube step, GCN-Polycube classification is used for polycube structure recognition. DL-Polycube employs multilayer perceptron (MLP)-based GCN-Polycube models, where MLPs serve as nonlinear regressors. The use of ReLU activation functions within these MLPs enhances the network’s nonlinear capabilities to fit complex patterns. This approach not only enables DL-Polycube to automatically

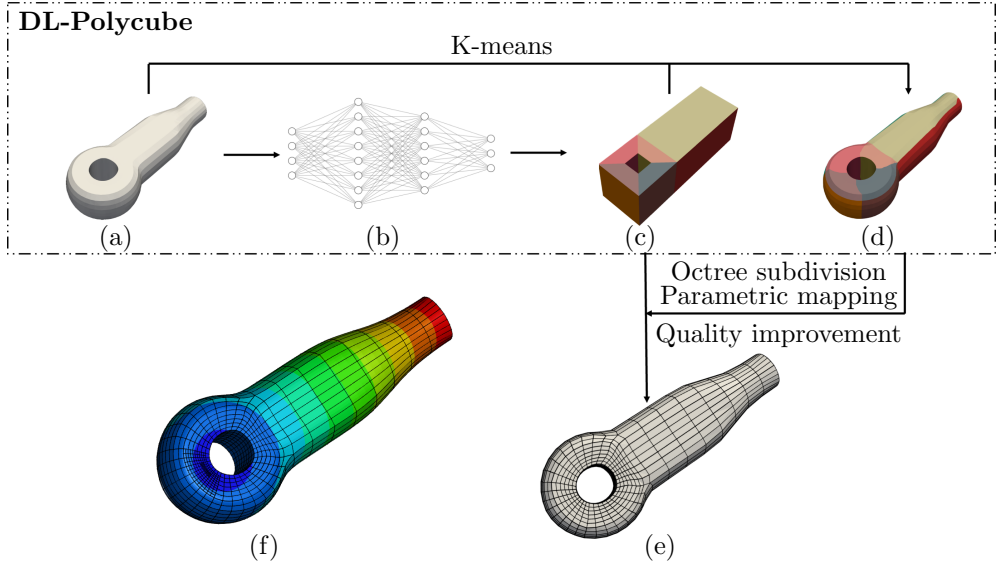


Fig. 1: The DL-Polycube pipeline using deep learning and the polycube method. (a) The CAD geometry and converting it into a triangular mesh; (b) a pretrained deep learning model to generate a polycube structure from the triangular mesh; (c) the polycube structure predicted by the deep learning model; (d) surface segmentation using the polycube structure information with K-means segmentation; (e) the polycube structure and surface segmentation are used to create an all-hex mesh through octree subdivision, parametric mapping and quality improvement techniques; and (f) volumetric spline with IGA simulation results using ANSYS-DYNA.

convert complex geometries into polycube structures, which ensures the generation of high-quality all-hex meshes, but also ensures rapid computations faster than traditional polycube-based methods [8, 22, 23, 28, 29, 42, 43].

During the training step, the ML model undergoes updates in polycube structure recognition and the K-means surface segmentation. The entire process eliminates the need for manual intervention, focusing instead on the efficient application of the trained model to new CAD geometries.

Regarding computational performance, generating and curating the dataset takes approximately 10 hours to produce 9,900 random meshes. Training the classification and regression networks for GCN-Polycube classification require an additional hour. During the prediction step, GCN-Polycube classification is completed in one second.

The DL-Polycube algorithm demonstrates its capability in rapidly predicting the corresponding polycube structure of geometric models and segmenting the surface of CAD geometry to achieve a one-to-one correspondence with the surface of the polycube structure. Consequently, this tool enables designers to convert boundary representation geometry into its corresponding polycube structure and facilitates automatic polycube-based hex mesh generation, as well as the construction of volumetric splines

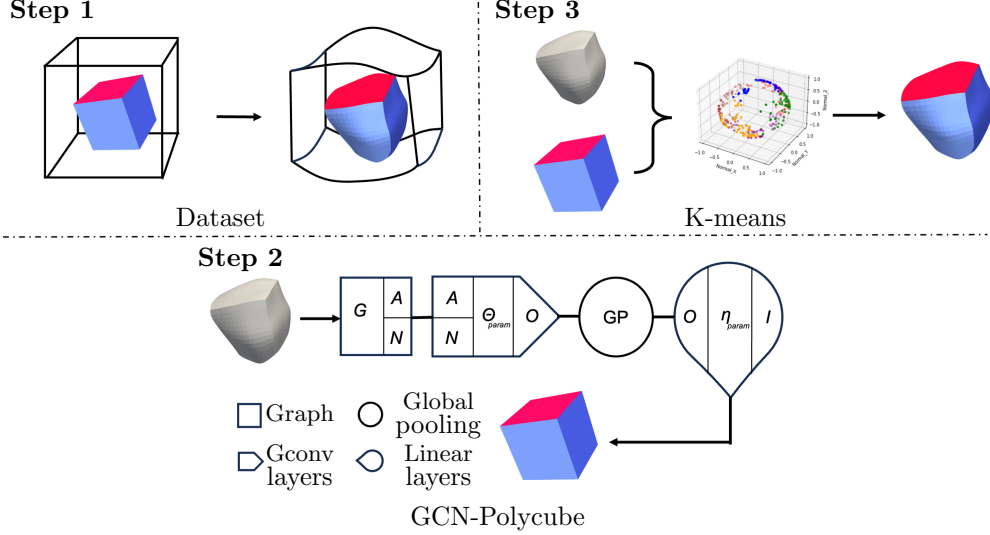


Fig. 2: Overview of the DL-Polycube algorithm. Step 1: Training dataset generation and curation: A cage is created around the target mesh to generate a diverse set of models with random transformations and deformations. Step 2: GCN-Polycube recognition: The GCN-Polycube classification enables the automatic conversion of complex geometries into polycube structures. Step 3: K-means surface segmentation: Segment the surface of CAD geometry to ensure a one-to-one correspondence with the surface of the polycube structure.

from CAD geometry. While DL-Polycube currently lacks parallel processing capabilities beyond the inherent parallelism of neural networks, its efficient computational framework makes it an important tool for creating polycube structures and generating hex meshes.

3 Implementation details of DL-Polycube

In the initial phase of our pipeline (see Fig. 1), we employ a pretrained model to convert CAD geometries into their corresponding polycube structures. Then, with the generated polycube structures and CAD models, we segment them into patches that have a one-to-one correspondence between the surface of the CAD and polycube structures. This process involves three key steps. Firstly, we generate “pseudo-random data” to establish a foundational relationship that links random surface triangular meshes with their corresponding polycube structures. Following this, a deep learning GCN-Polycube model architecture, is trained using the pseudo-random data and their corresponding polycube structures from the first step. This step learns the mapping between triangular meshes and polycube structures. Finally, we use the K-means clustering method, which is based on spatial attributes such as normal vectors and centroids obtained based on the polycube structures. This method segments the

surface by classifying each triangular element into one patch. This entire process aims at automatically achieving surface segmentation and its corresponding polycube structure.

3.1 Dataset generation and curation

3.1.1 Procedural geometric modeling

We use the 3D graphics software Blender, along with its built-in Python and BMesh libraries, to create polycube structures and a wide range of derivative geometries resulting from their transformations and deformations. These derivative geometries and their corresponding polycube structures are used as inputs and outputs for our deep learning model system. This procedural geometric model employs a multi-step strategy to compute the polycube structures and their derivative geometries. The first step involves using Boolean operations to generate polycube structure, as illustrated in Fig. 3. The second step involves surface subdivision using the Catmull-Clark algorithm, followed by triangulation of the generated polycube structures. The third step involves free-form deformation. This procedural geometric modeling process is configured to produce polycube structures and subsequent derivative geometries. Starting with a polycube structure in the first step, the second and third steps generate 900 derivative geometries corresponding to each initial polycube structure. Thus, the entire procedural geometric modeling process generates the input and output data for training.

Finally, we employ procedural geometric modeling to obtain eleven types of polycube structures and their derivative geometries. These polycube structures correspond to configurations of a single cube, a genus-one cube, and combinations of these two primitive geometries. For each type of polycube structure, we generate 900 corresponding derivative geometries. Note that we only generate eleven polycube structures as a proof of concept. One can generate more polycube structures to make the pipeline work for other types of geometries.

3.1.2 Data generation

We employ a parametric script to create various polycube designs, often starting with basic shapes like cuboids. This script begins by using Boolean operation to combine basic shapes into a polycube structure and then alters its transformation and deformation behaviors through procedural geometric modeling, as mentioned in the previous section. Consequently, the resulting geometry exhibits diverse shapes and transformation and deformation behaviors while maintaining topological consistency. It is important to note that the variability of the design parameters constrains the generalizability of the machine learning model. If the geometry model encounters design parameters outside its trained range, it is likely to yield less accurate results. Therefore, these factors must be considered and integrated throughout the entire pipeline when developing a model for automatically generating hex meshes.

We use a cuboid primitive with a hole (genus-1) as an example to illustrate our process (see Fig. 3). Firstly, we create the cuboid primitive with a hole using Boolean operation. Then, we refine it through surface subdivision using the Catmull-Clark

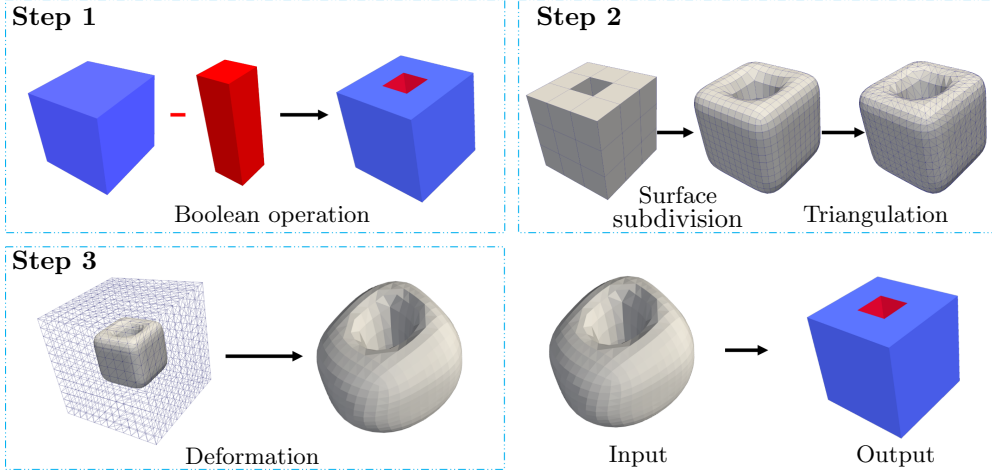


Fig. 3: Procedural geometric modeling process of GCN-Polycube model architecture. Step 1: Initial polycube structure created using Boolean operations. Step 2: Surface subdivision applied using the Catmull-Clark algorithm and triangulation of the subdivided surface. Step 3: Free-form deformation applied to the triangulated and subdivided polycube structure. These steps generate input and output geometries for deep learning model training.

algorithm in Blender. Next, we convert it into a triangular mesh through triangulation and scale it to a specified size. It is important to note that scaling to a specified size can play an important role in feature scaling during model training. Subsequently, we surround the cuboid with a hole with a cage and apply random stretching to achieve random deformations of the basic mesh. Finally, these random meshes serve as inputs for training the neural network in the subsequent reverse process.

3.1.3 Feature extraction

The deformed geometries derived from the initial polycube structures are used for feature extraction to create the training dataset. Given an input surface triangular mesh T from the derivative geometry, the geometry can be represented as an abstract graph $G = (A, N)$, where the adjacency matrix $A = \{A_{ij}\}_{i=1\dots N_n, j=1\dots N_n}$ defines the connectivity between triangular elements, with $A_{ij} = 1$ indicating that two triangular elements are adjacent. The node feature vectors $N = \{N_i\}_{i=1\dots N_n}$ encode the characteristics of each triangular element. Each node feature vector includes details of the triangular element, such as the vertices that form it and 3D position \mathbf{p} of each vertex $v_i \in \mathcal{V}$:

$$\mathbf{p}_i := \mathbf{p}(v_i) = \begin{pmatrix} x(v_i) \\ y(v_i) \\ z(v_i) \end{pmatrix} \in \mathbb{R}^3. \quad (1)$$

Besides the physical information, the node feature vectors $N = \{N_i\}_{i=1\dots N_n}$ also include additional attributes such as the normal vector of each face. This dataset,

which includes detailed geometric and topological information, is designed for GCN-Polycube classification and K-means surface segmentation.

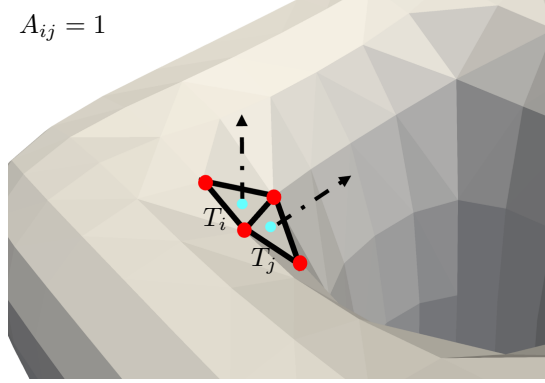


Fig. 4: Feature extraction and data integration process for GCN-Polycube classification and K-means surface segmentation. $A_{ij} = 1$ indicating that two triangular elements i and j are adjacent. The node feature vectors N include vertex coordinates (red points), centroid coordinates (yellow points), and normal vectors (dashed arrows) of each face.

With the data generated and features extracted, we begin with data labeling. All derivative geometries are generated through the polycube structure, which automatically assigns the types of polycube structures as labels to the existing data. As a result, these derivative geometries and their corresponding polycube structures serve as inputs and outputs for our deep learning model. Next, we perform data curation. We collect and merge data from multiple sources, including the normal vector in normal space, the vertex coordinates and the centroid coordinates of triangular elements in 3D Euclidean space, and the adjacency matrix of the graph (see Fig. 4). We use these data as features. These features include various geometric and graph information to help our models learn and predict more effectively.

3.2 Machine learning model

The DL-Polycube algorithm aims to automatically generate polycube structures and ensure a one-to-one correspondence between the surface of CAD geometry and polycube structures. To achieve this, we will first use GCN-Polycube to extract the polycube structure of the CAD geometry. Based on the algorithm, the possible corresponding polycube structures will be given. Then, we will use K-means segmentation to perform surface segmentation.

3.2.1 GCN-Polycube model architecture

Fig. 5 provides a hierarchical overview of the GCN-Polycube model architecture. The architecture is composed of multiple layers designed to capture and process the spatial

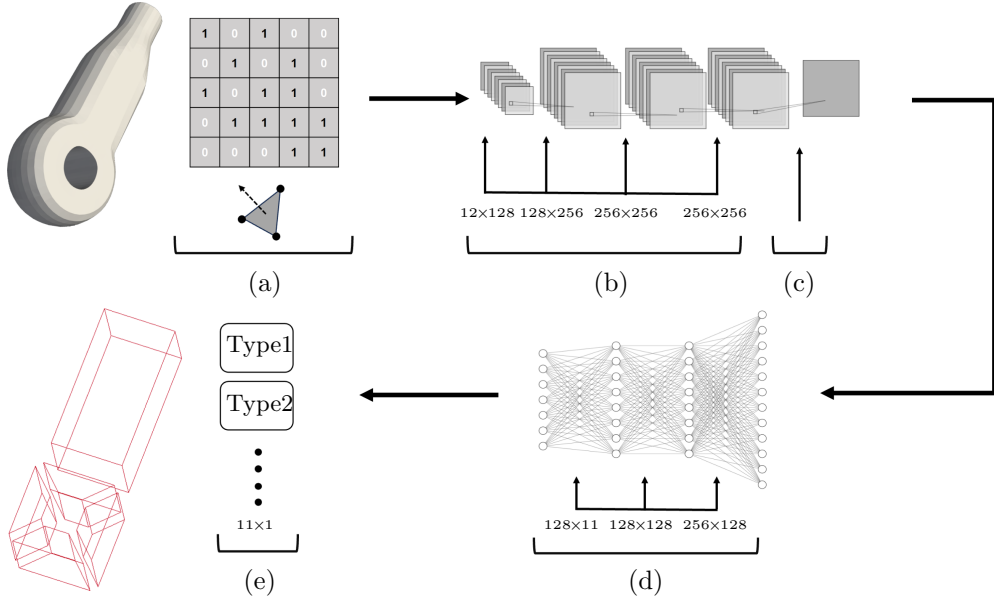


Fig. 5: Hierarchical overview of the GCN-Polycube model architecture. (a) The input features from the CAD geometry. (b) The four GCN-Polycube layers capture local and global geometric structures. (c) The pooling layer aggregates node-level information into graph-level representations. (d) The fully connected layers map the features of complex topological structures to the target space, i.e., the polycube structure. (e) The output predicts the suggest corresponding polycube structures.

relationships and features of the deformed geometries derived from the initial polycube structures. The initial layer takes the graphical representation of the CAD geometry as input, transforming it into a feature-enhanced representation through convolutional operations that consider both node features and their connections. Subsequent layers in the GCN-Polycube further refine these features by aggregating information from neighboring nodes, capturing the local and global geometric structures. This hierarchical processing allows the model to understand complex spatial dependencies and interactions within the CAD geometry. The output of the GCN-Polycube is then used to suggest possible corresponding polycube structures, ensuring a one-to-one correspondence between the surface of the CAD and polycube models. A layer of a GCN-Polycube can be described by the following formula [44]:

$$F^{(l+1)} = H \left(\tilde{D}^{-1/2} \tilde{A} \tilde{D}^{-1/2} F^{(l)} W^{(l)} \right), \quad (2)$$

where $F^{(l)}$ represents the feature matrix at layer l , $\tilde{A} = A + I$ is the adjacency matrix of the graph with added self-loops, \tilde{D} is the degree matrix of \tilde{A} , $W^{(l)}$ is the trainable weight matrix of layer l , and H is the activation function ReLU. Our neural network consists of those four GCN-Polycube layers followed by a global average pooling,

concluding with a fully connected layer to produce the output. The Algorithm 1 is a snippet of the forward computation of a GCN-Polycube Layer.

Algorithm 1 Forward computation of GCN-Polycube layer

- 1: **Input:** Feature matrix $F^{(l)}$, Adjacency matrix A , Weight matrix $W^{(l)}$
 - 2: **Output:** Updated feature matrix $F^{(l+1)}$
 - 3: Add self-loops to adjacency matrix of deformed geometries derived from the initial polycube structures
 - 4: Compute degree matrix of deformed geometries
 - 5: Compute inverse square root of degree matrix
 - 6: Normalize adjacency matrix
 - 7: Linear transformation of normalized adjacency matrix
 - 8: Apply activation function to transformation result
 - 9: **return** $F^{(l+1)}$
-

Loss function in GCN-Polycube. The loss function quantifies the difference between the predicted polycube structures and the true polycube structures (initial polycube structures in Sec. 3.1.1). For GCN-Polycube, we use the cross-entropy (CE) loss, which measures the performance of our GCN-Polycube model. The CE loss is defined as:

$$\mathcal{L}_{\text{CE}} = -\frac{1}{N} \sum_{i=1}^N \sum_{c=1}^C y_{i,c} \log(\hat{y}_{i,c}) + \lambda \sum_l \|W^{(l)}\|^2, \quad (3)$$

where N is the number of training data, C is the number of types of polycube structure considered in this paper, $y_{i,c}$ is the binary indicator indicating whether the true polycube structure c is the correct classification for training data i , and $\hat{y}_{i,c}$ is the predicted probability that training data i belongs to true polycube structure c . L_2 regularization is adopted to prevent overfitting. Here λ is a regularization parameter that controls the trade-off between fitting the data and keeping the model weights small, and $W^{(l)}$ are the weights of the l -th layer shown in Equation (2).

3.2.2 K-means model architecture

Step 3 in Fig. 2 provides a hierarchical overview of the model architecture for K-means surface segmentation using polycube structure information. By using a trained GCN-Polycube model from the previous step, we can obtain the predicted polycube structure of the CAD geometry. Subsequently, we use the K-means algorithm to segment the CAD geometry into k clusters in an unsupervised manner. Traditionally, the number of clusters k in K-means is a hyperparameter. However, in this context, k is known because it corresponds to the k faces of the predicted polycube structure. The k initial centroids are not chosen randomly; instead, they are calculated by taking the mean of the normal vectors corresponding to the predicted polycube structure. We first select k initial centroids based on the predicted polycube structure. Each normal vector of a face of predicted polycube structure is used as an initial centroid. Given an input surface triangular mesh T from CAD geometry, let the dataset $X = \{x_{T(i)}\}_{i=1}^n$

denotes the unit normal vectors $x_{T(i)}$ set of the triangular mesh in the normal space, where n is the total number of triangles and $T(i)$ represents the i^{th} triangle in the physical space. Then we assign each data point $x_{T(i)}$ to the nearest centroid based on the Euclidean distance in the normal space. This can be expressed as:

$$C_j = \{x_{T(i)} : \|x_{T(i)} - \mu_j\|^2 \leq \|x_{T(i)} - \mu_l\|^2 \ \forall l, 1 \leq l \leq k\}, \quad (4)$$

where C_j is the set of points assigned to centroid μ_j . Then we recalculate the centroids as the mean of all data points $x_{T(i)}$ assigned to each cluster:

$$\mu_i = \frac{1}{|C_j|} \sum_{x_{T(i)} \in C_j} x_{T(i)}, \quad (5)$$

where $|C_j|$ is the number of points in cluster C_j . Finally, we repeat the assignment and update steps until the loss function no longer change significantly (<3%). The loss function is defined as:

$$\sum_{j=1}^k \sum_{x_{T(i)} \in C_j} \|x_{T(i)} - \mu_j\|^2. \quad (6)$$

This results in k clusters and surface of geometry is segmented into k parts corresponding to the polycube structures. Algorithm 2 is a snippet of the K-means Clustering Algorithm combined with polycube structure information.

Algorithm 2 K-means clustering algorithm

- 1: **Input:** Manifold, watertight triangular mesh T , number of clusters k obtained from the initial polycube structure, data points $x_{T(1)}, x_{T(2)}, \dots, x_{T(n)}$, the normal vector of each surface of polycube structure $\mu_1, \mu_2, \dots, \mu_k$
 - 2: **Output:** Surface segmentation results
 - 3: Initialize k centroids of data as $\mu_1, \mu_2, \dots, \mu_k$
 - 4: **repeat**
 - 5: **Assignment step:**
 - 6: **for** each data point $x_{T(i)}$ **do**
 - 7: Assign $x_{T(i)}$ to the cluster C_j with the nearest centroid
 - 8: **end for**
 - 9: **Update step:**
 - 10: **for** each cluster C_j **do**
 - 11: Update the centroid μ_j to the mean of all points in C_j
 - 12: **end for**
 - 13: **until** centroids do not change significantly
 - 14: Obtain cluster assignment for each data point and its corresponding cluster centroid
 - 15: Cluster assignments lead to surface segmentation
-

3.3 Model training in GCN-Polycube and K-means

In our study, the MLP within the GCN-Polycube model consists of three hidden layers with widths (256, 128, 128). We train the GCN-Polycube model as a deep network using batch gradient descent and the Adam optimizer. Subsequently, we determine the learning rate of our method through a hyperparameter search (as shown in Fig. 6(a)). Through this analysis, we identify the optimal hyperparameter setting that result in the smallest error. Fig. 6(b) displays the model’s accuracy over epochs, indicating the improvement in model performance through training, while Fig. 6(c) illustrates the loss function of the GCN-Polycube model as a function of epochs, demonstrating the convergence behavior during training. In the training process of the K-means model, the iteration stops when the centroids no longer change significantly (as depicted in Fig. 6(d)).

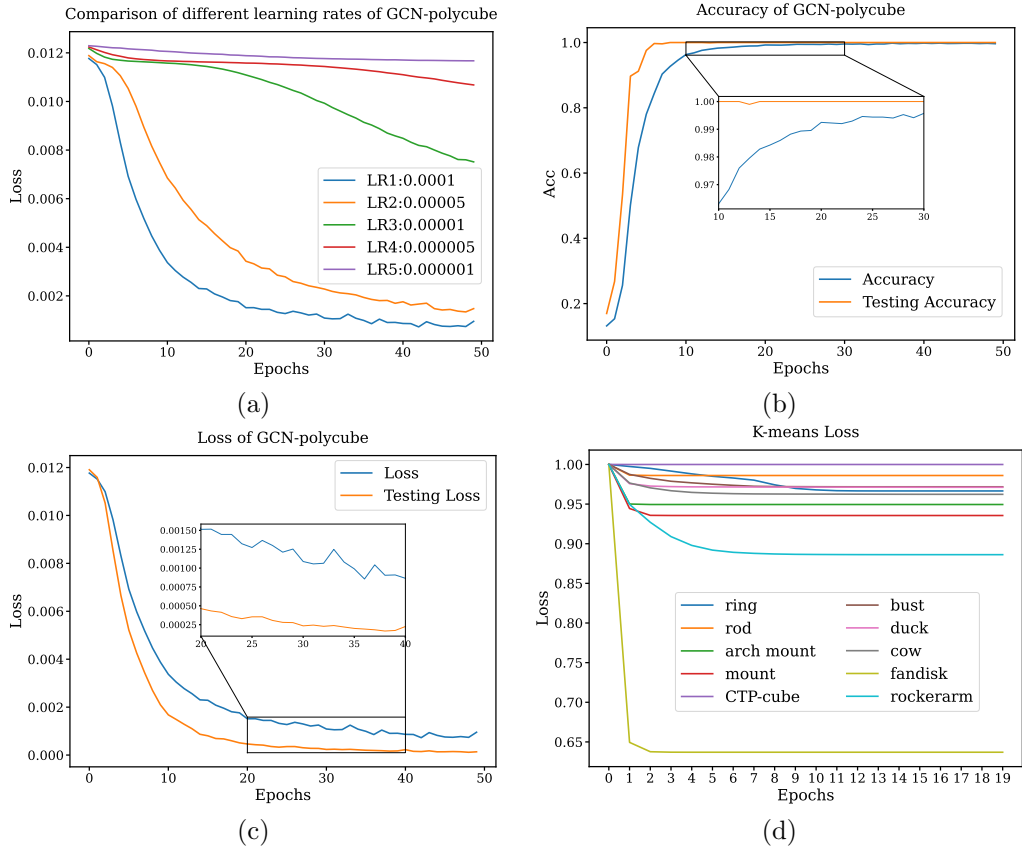


Fig. 6: Hyperparameter optimization and training performance of the GCN-Polycube model and K-means model. (a) Hyperparameter search results for learning rates. (b) Accuracy of the GCN-Polycube model as a function of epochs. (c) Loss of the GCN-Polycube model as a function of epochs. (d) Loss of the K-means model.

4 ML-Polycube based segmentation and path optimization

This section introduces the pipeline of integrating polycube structure information with K-means segmentation and path optimization to produce high-quality surface segmentation to match the polycube structure. In the K-means step from the previous section, a significant challenge arises from the need to segment not only based on the normal space but also based on 3D Euclidean space. It is common for two regions on the polycube structure to lie on the same plane (see Fig. 7(b)). To accurately segment these regions, especially when they are co-planar, it is important to determine the approximate location of each cluster. This requires K-means segmentation to be performed in both the normal space and a space formed by the centroids of the triangular elements. A secondary GCN model (GCN-centroid) is employed to predict the centroids when regions lie on the same plane but are separated in the polycube structure. After segmentation based on the polycube structure is introduced, the next challenge is the zigzag issue, as illustrated in Fig. 7(c). To address this problem, we use a polycube-based Dijkstra’s shortest path algorithm. The final outcome is a one-to-one correspondence between the segmented surface and the surface of the polycube structure.

4.1 GCN-based centroid prediction for surface segmentation

In the K-means step, the predicted polycube structure is used to determine the number of clusters for the K-means algorithm. To segment the surface more accurately, especially when two regions lie on the same plane and cannot be distinguished using only the normal space, we use a space formed by the centroids of the triangular elements. A GCN-centroid model is then employed to predict these centroids. The GCN-centroid is trained to recognize and predict the centroids based on the polycube structure, enabling the K-means algorithm to determine the approximate location of each cluster according to the polycube structure.

Similar to the GCN-Polycube used in polycube structure recognition, we first perform feature extraction. Here, we calculate the centroid of a triangular element based on its 3D position vector \mathbf{p} of each vertex $v_i \in \mathcal{V}$. Then we use the centroid of a triangular element as the node feature vector. The layers of the GCN-centroid can be described by Equation (2), where $F^{(l)}$ represents the feature matrix corresponding to the centroid of a triangular element.

The model architecture includes four GCN-centroid layers that capture and refine node features, which are the centroids, followed by global max pooling to aggregate these features. Subsequent linear layers further process the pooled features to predict the centroids. We train the GCN-centroid model using batch gradient descent. Although both the Adam and RMSprop optimizers are suitable for this task, we choose to use the RMSprop optimizer.

The predicted centroids are then used for K-means surface segmentation based on 3D Euclidean space. These segmentation used in conjunction with the K-means algorithm based on the normal space to segment the surface into k clusters, corresponding to the polycube structure. The initial centroids for K-means are selected based on the

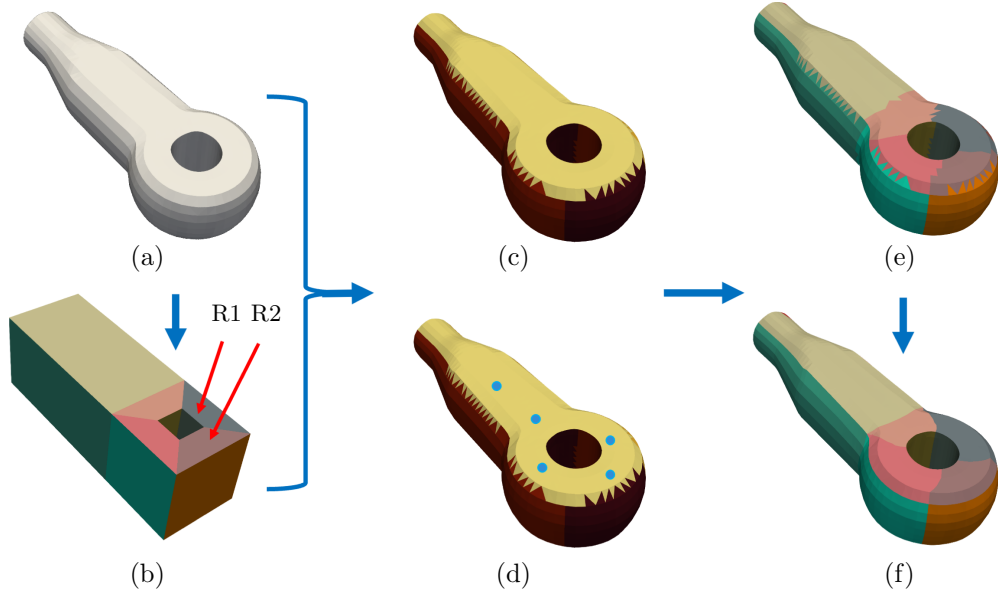


Fig. 7: Surface segmentation using K-means clustering based on predicted polycube structure and GCN-centroid model. (a) The CAD geometry; (b) initial polycube structure prediction used to determine the number of clusters and two regions (R1 and R2), where “R” stands for “Region”, lie on the same plane within the polycube structure; (c) K-means clustering based on the normal space and the zigzag issue during segmentation; (d) feature extraction and centroid prediction using the GCN-centroid model; (e) K-means clustering in 3D Euclidean space using predicted centroids; (f) final optimized segmented surface.

predicted polycube structure. The K-means segmentation process involves assigning each triangular element to the nearest centroid based on Euclidean distance, followed by iterative refinement of the centroids. The mathematical equation and algorithm are similar to Equation (4) and Algorithm 2, but with the normal space replaced by a space formed by the centroids of the triangular elements.

4.2 Dijkstra’s algorithm for zigzag path optimization

After segmenting the mesh using K-means, we often encounter zigzag issues in the generated segments. To address this, we use Dijkstra’s shortest path algorithm to optimize the paths. The algorithm considers the geometric properties of the edges, such as length and angles, to ensure smooth and accurate paths. By minimizing the cumulative edge weights, the algorithm finds the shortest path in a graph. Let $g = (v, e)$ be a graph with vertices v and edges e , and let $w(e)$ be the weight of edge e .

The shortest path from vertex v_i to vertex v_j is determined by:

$$\text{dist}(v_i, v_j) = \min_{\text{paths } v_{ij}} \sum_{e \in v_{ij}} w(e). \quad (7)$$

The path finding process involves edge weight adjustment. This adjustment ensures that the paths found not only minimize distance but also conform to the desired geometric constraints, such as the sharp features in the original geometry. Here, the edge weight is adjusted as follows. For an edge e between vertices v_i and v_j , the weight $w(e)$ is calculated as:

$$w(e) = \frac{1}{\lambda_0} \|\mathbf{v}_i - \mathbf{v}_j\| + \lambda_1 \theta + \lambda_2 \phi, \quad (8)$$

where $\|\mathbf{v}_i - \mathbf{v}_j\|$ is the Euclidean distance. The coefficient λ_0 depends on whether the edge is a sharp feature or not. This adjustment allows the influence of sharp features to be incorporated based on the edge length. The second term θ considers the direction of the current edge relative to the previous edge. The third term ϕ controls the direction of the selected edge so that it does not deviate from the overall direction from the origin to the destination node. The coefficients λ_1 and λ_2 are penalty coefficients. This optimization step ensures that the final segments align well with the polycube structure and thus eliminates the zigzag problem.

Fig. 8 provides a detailed overview of the algorithm used to determine the shortest path between corner nodes. The process begins by identifying corner nodes based on polycube structure, which are then used to define pairs of points representing potential edges. These corner pairs are stored and used to guide the pathfinding process. The algorithm iteratively explores paths from a starting vertex to a target vertex, updating the shortest known path to each vertex encountered.

Once a path is found, the edges along this path are marked and stored, preventing their reuse in subsequent iterations. This ensures that each edge is uniquely assigned to a path, avoiding overlaps and intersections. The resulting paths are then used to update the surface segmentation (see Fig. 7(e) and (f)).

5 High-quality hex mesh generation and volumetric spline construction

5.1 Octree subdivision and parametric mapping

Upon the polycube is predicted by the GCN-Polycube algorithm and the surface is segmented by the K-means, we need to build a bijective mapping between the input triangular mesh and the boundary surface of the polycube structure. Our implementation adopts the strategy proposed in [42], utilizing an union of unit cubes as the parametric domain for the polycube structure (see Fig. 9). The integration of the segmented surface mesh (provided by K-means) and the polycube structure (provided by GCN-Polycube) yield a parametric domain to perform the following octree subdivision and parametric mapping; see the pseudocode provided in the Parametric mapping algorithm [24].

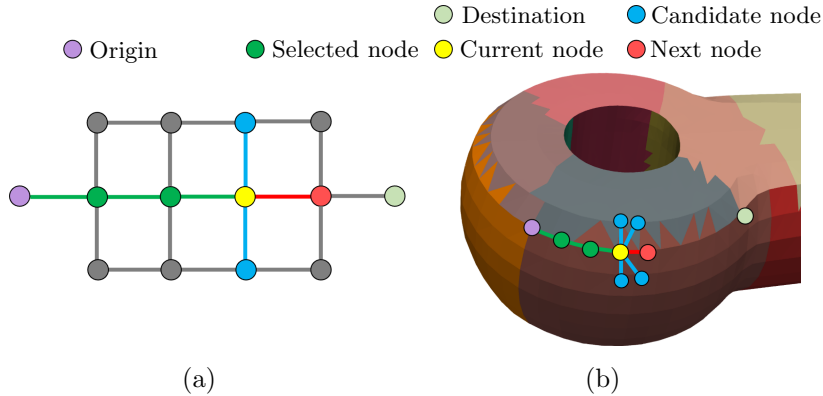


Fig. 8: Pathfinding optimization using Dijkstra’s algorithm to address zigzag issues in generated segments. (a) Identification of corner nodes based on the polycube structure, with a diagram illustrating the origin and destination nodes; (b) definition of potential edges between corner nodes. Calculation of edge weights considering Euclidean distance, angle with reference direction, and additional penalty terms.

Let $\{S_i\}_{i=1}^N$ be the segmented surface patches, derived from the segmentation result by K-means (see Fig. 9(a)). Each segmented surface patch corresponds to one boundary surface of the polycube P_i ($1 \leq i \leq N$), as shown in Fig. 9(b), where N represents the number of the boundary surfaces. Additionally, the polycube includes internal surfaces marked as I_j ($1 \leq j \leq M$), with M being the number of the interior surfaces. Then, the collective set of polycube surfaces consists of $\{P_i\}_{i=1}^N$ and $\{I_j\}_{j=1}^M$, which can be obtained automatically from the polycube structure derived from the GCN-Polycube. For the parametric domain, let $\{U_k\}_{k=1}^6$ denote the six surface patches of one unit cube (see Fig. 9(b)).

Each cubic region within the polycube structure corresponds to a distinct volumetric region of the geometry and is paired with a unit cube as its parametric domain. The representation of a cubic region and its associated geometric volume region, highlighted by a dashed rectangle, is shown in Fig. 9(b). Therefore, for each cube in the polycube structure, there is a boundary surface P_i to which the segmented surface patch S_i is mapped onto the corresponding parametric surface U_k of the unit cube. The mapping process from S_i to U_k begins by mapping the boundary edges of S_i with those of U_k . We then determine the parameterization of S_i by using the cotangent Laplace operator to solve for the harmonic function [8, 45]. It is important to note that the parametric mapping step is omitted for the internal surfaces I_j of the polycube.

An all-hex mesh is generated from this surface parameterization coupled with octree subdivision. For each cubic region, vertex coordinates on the segmented patch S_i are first determined by recursively subdividing the unit cube to acquire their parametric coordinates. The physical coordinates are then obtained via the parametric mapping, ensuring a bijective relation between the parametric domain U_k and the physical domain S_i . To locate vertices on the internal surface of the cubic section,

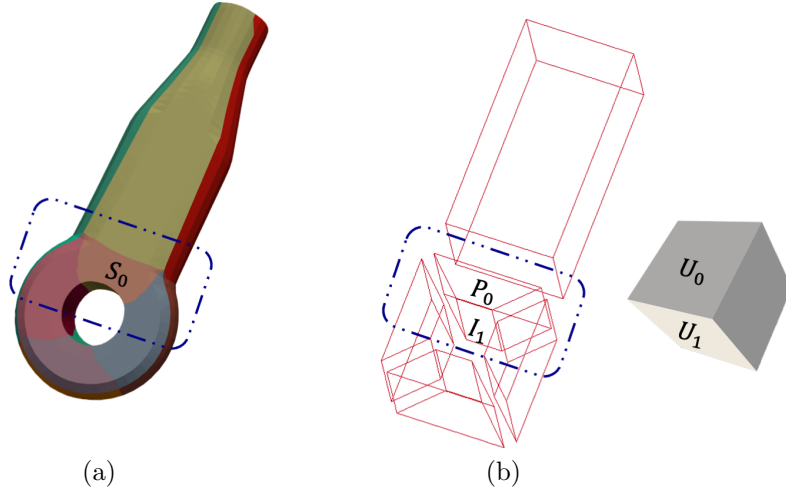


Fig. 9: The parametric mapping process for constructing an all-hex mesh using a pre-icated polycube structure. (a) The segmented surface patches $\{S_i\}_{i=1}^N$ derived from the K-means segmentation; (b) the polycube structure $\{P_i\}_{i=1}^N$ and internal surfaces $\{I_j\}_{j=1}^M$ with each cubic region corresponding to a unit cube $\{U_k\}_{k=1}^6$ as the parametric domain. The dashed rectangle highlights the correspondence between a cubic region in the polycube and its associated geometric volume.

linear interpolation is used to compute the physical coordinates directly. The mappings among S_0 , P_0 , and U_0 are combined to establish the parametric mapping and to determine vertex coordinates on the surface S_0 . The internal surface I_1 is paired with U_1 for linear interpolation to calculate the vertices on the internal surface of the cubic section. Lastly, vertices within the cubic region are derived through linear interpolation. The complete all-hex mesh is constructed by iterating over each cubic region.

This robust component of the system, HexGen, which is part of the HexGen_Hex2spline subroutine, has been made publicly accessible via GitHub (https://github.com/CMU-CBML/HexGen_Hex2Spline.git). It comes with comprehensive documentation and references [24] for an in-depth understanding.

5.2 Quality metrics and quality improvement

Mesh quality is important in both FEA and IGA, as poor quality elements can compromise the convergence and stability of simulations. Unfortunately, meshes generated through the previous parametric mapping step frequently exhibit poor-quality elements. In this section, we will present one quality metric we take into account and three algorithms we employ for improving mesh quality.

We evaluate mesh quality based on the scaled Jacobian [46]. For each hex element, we identify three edge vectors $e_i = x_i - x$ ($i = 0, 1, 2$) for every corner node x . The Jacobian matrix at x is defined as $[e_0, e_1, e_2]$, and its Jacobian $J(x)$ is the determinant of this matrix. We derive the scaled Jacobian $SJ(x)$ by normalizing e_0, e_1 and e_2 . For

each hex element, we compute the (scaled) Jacobian at eight corners and the body center. For the body center, e_i ($i = 0, 1, 2$) are determined using three pairs of opposite face centers.

We integrate three quality improvement techniques in the software package, namely pillowing, smoothing and optimization. Note that each quality improvement function can be run independently and one can use these functions to improve the mesh quality. We first use pillowing to insert one layer around the boundary [8]. By using the pillowing technique, we ensure that each element has at most one face on the boundary, which can help improve the mesh quality around the boundary. To improve the mesh quality, pillowing, smoothing, and optimization are alternately employed [8, 39]. This process involves moving the vertices while ensuring that the boundary points remain on the input triangle surface. In each iteration, optimization is carried out to the element with the worst-scale Jacobian in the entire mesh and make adjustments to its corner nodes. Additionally, Laplacian smoothing is applied to all vertices every 1,000 iterations to ensure a smooth vertex distribution.

For smoothing, different relocation methods are applied to three types of vertices: vertices on sharp edges of the boundary, vertices on the boundary surface, and interior vertices. We perform smoothing on the surface before smoothing the interior volume. For each sharp-edge vertex, we first detect its two neighboring vertices on the curve, and then calculate their middle point. For each vertex on the boundary surface, we calculate the area center of its neighboring boundary quadrilaterals. For each interior vertex, we calculate the weighted volume center of its neighboring hex elements as the new position. We relocate a vertex in an iterative way. Each time the vertex moves only a small step towards the new position and this movement is done only if the new location results in an improved local scaled Jacobian.

In the optimization process, we observe that optimizing purely on the scaled Jacobian function leads to gradient explosion and entrapment in local minima [39]. Although optimizing purely with the Jacobian function can solve these two problems, we cannot assess the ideal shape of an element once the Jacobian value transitions to positive [39]. Therefore, we adopt a new energy function, consisting of the geometry fitting, Jacobian, and scaled Jacobian terms. We have

$$E = \sum_{i=0}^{nm_s-1} \|x_i - x_i^s\|_2^2 - \frac{1}{\bar{l}} \sum_{j=0}^{ne_n-1} \min J(h_j) - \bar{l}^2 \sum_{k=0}^{ne_p-1} \min SJ(h_k), \quad (9)$$

where nm_s is the number of surface vertices, ne_n is the number of hex elements with negative Jacobians, ne_p is the number of hex elements with positive Jacobians, and \bar{l} is the average length of three edges to calculate the (scaled) Jacobian. Let us assume the fundamental dimension of geometric length is L . Then the dimension of the geometry fitting term is L^2 , the Jacobian and the scaled Jacobian are in the dimension of L^3 and L^0 , respectively. To unify the dimension of the Jacobian and scaled Jacobian terms to L^2 , we introduce $\frac{1}{\bar{l}}$ to the Jacobian term and \bar{l}^2 to the scaled Jacobian term. We adopt the gradient-based method to iterative minimize the energy function. All the

mesh vertices are optimized by

$$x_i \rightarrow x_i - \alpha \nabla E_{x_i}, \quad i = 0, 1, \dots, nn - 1, \quad (10)$$

where nn is the number of all vertices. We choose the weight $\alpha = 1 \times 10^{-4}$ for all the tested models in this paper.

To efficiently determine the nearest surface point x_i^s for each boundary point x_i , we check all triangles within a bounding box ten times the length of the local triangular edge. The identification process for x_i^s varies depending on whether x_i is projected onto a face, edge, or point. If x_i is projected onto a face, we iterate through all triangles in the bounding box, calculate the point-to-triangle distance, and determine the nearest projection point x_i^s . In contrast, if x_i is directly projected onto a point, x_i^s simply becomes that point. If x_i is projected onto an edge, x_i^s is searched on the corresponding sharp edges in the triangle mesh. To expedite the process, we update the closest triangle index for each x_i every 1,000 iterations. If the maximum of the minimum distances from all points to the surface is less than 10^{-8} of the overall bounding box edge size, we directly pull each x_i to its corresponding x^s . We present Algorithm 3 for the entire quality improvement pipeline.

Algorithm 3 Quality Improvement Algorithm

```

1: Input: Manifold, watertight triangular mesh  $T$  with annotated sharp features, an
   all-hex mesh  $\mathcal{H}$  to be fitted to  $T$ 
2: Initialize  $N \leftarrow \#elem \in \mathcal{H}, \alpha \leftarrow 10^{-4}$ 
3: for  $x_i \in \mathcal{H}$  surface do
4:   if  $x_i$  is closest to a corner node then
5:     Classify  $x_i$  as a corner node
6:   else if A* algorithm determines  $x_i$  is along a shortest path then
7:     Classify  $x_i$  as an edge point
8:   else
9:     Classify  $x_i$  as a face point
10:  end if
11: end for
12: while minimum scaled Jacobian < given threshold do
13:   Calculate  $x_i^s, \forall x_i \in \mathcal{H}$  surface
14:   // Gradient-Based Mesh Quality Optimization
15:    $g \leftarrow \nabla E_{x_i}$ 
16:    $x_i \leftarrow x_i + \alpha g$  ▷ Update vertex position based on Jacobian
17:   // Laplacian Smoothing
18:   if iter % 1000 == 0 then
19:     smartLaplacianSmoothing( $\mathcal{H}$ ) ▷ Smooth vertex position
20:   end if
21:   iter  $\leftarrow$  iter + 1
22: end while
23: return  $\mathcal{H}$ 

```

5.3 Hex2Spline: volumetric spline construction

Upon acquiring the hex mesh of satisfactory quality, the subsequent step involves constructing the volumetric spline, specifically the TH-spline3D, on these unstructured hex meshes. This process consists of two steps: the construction of TH-spline3D on hex meshes and the extraction of Bézier elements for IGA simulation in ANSYS-DYNA. Our previous software, Hex2Spline, uses a generated hex mesh as the input control mesh to facilitate the construction of a TH-spline3D over CAD geometry. This robust portion of the system has been made publicly accessible via GitHub (https://github.com/CMU-CBML/HexGen_Hex2Spline.git), complete with comprehensive documentation and reference [24, 31] for an in-depth understanding. Capable of defining spline functions over arbitrarily unstructured hex meshes, Hex2spline supports sharp feature preservation, and global refinement (see Fig. 10(a)), Hex2spline also incorporates adaptive IGA with its local refinement capabilities (see Fig. 10(b)). Hex2Spline can output the Bézier information of constructed volumetric splines for IGA simulation in ANSYS-DYNA or alternative IGA platforms.

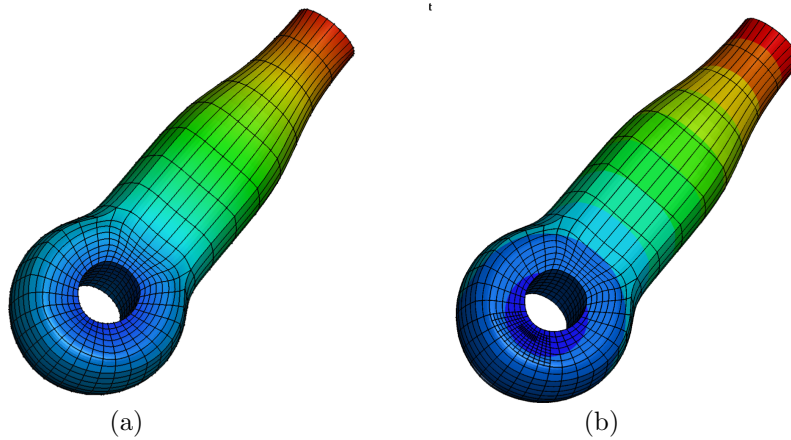


Fig. 10: Visualization of the output Bézier mesh with: (a) global refinement and (b) two levels of local refinement with IGA eigenvalue analysis in ANSYS-DYNA.

6 Results

In this section, we demonstrate the effectiveness and robustness of the DL-Polycube algorithm through various test cases. We evaluate the performance of our approach on a range of CAD geometries with varying complexities and topologies. The results are analyzed in terms of polycube structure prediction accuracy, and the overall quality of the generated hex meshes and IGA results.

6.1 Dataset of deep learning models

The training process for the deep learning models is conducted using a large dataset of generated geometric models. The dataset includes a wide variety of polycube structures and their corresponding deformed geometries, ensuring diverse training examples. The dataset was generated using Blender and its built-in Python and BMesh libraries. We created 11 types of polycube structures, each with 900 derivative geometries, resulting in a total of 9,900 training examples. Fig. 11 displays the dataset, including the polycube structure and their derivative geometries, with two randomly chosen examples.

6.2 Polycube structure prediction

We tested the DL-Polycube algorithm on a set of 16 CAD models, including mechanical parts and free-form geometries. We applied deep learning to classify the polycube structures of these 16 models in order to determine the most likely polycube structure. The accuracy of polycube structure prediction was evaluated by comparing the predicted structures with the constructed ground truth polycube structures. The probability distributions output by the model are shown in Table 1. To clarify, we have named Type-1 as the P1 column, Type-2 as the P2 column, Type-3 as the P3 column, and so on. The order of types corresponds to Fig. 11. The probability distribution represents the model’s confidence in how well the predicted polycube structure matches each type of the ground truth. Specifically, for the rod model, the probability for P3 (Type-3) is 100.00%, which indicates that the model believes the predicted structure most likely belongs to Type-3. The surface triangle meshes with predicted polycube structures for these models are shown in Figs. 12, 13, 14, and 15. Interestingly, the probability distribution of predicted polycube structures shows that some models can potentially match multiple polycube structures. In such cases, we select the polycube structure corresponding to the highest probability. For example, in the case of the dice model, it has a 65.13% probability for P1 (Type-1), but also a 34.6% probability for P6 (Type-6). Here, we choose the structure with the highest probability, which is Type-1.

6.3 Hex mesh generation and volumetric spline construction

The Polycube structure prediction and surface segmentation are performed using the DL-Polycube program. The DL-Polycube algorithms are implemented in Python using the PyG library [47]. The software is open-source and available at the following GitHub repository: <https://github.com/CMU-CBML/DL-polycube>. The hex mesh generation and volumetric spline construction are done with the help of two software packages: Hex2Gen and Hex2Spline. These packages are open-source and available at the following GitHub repository: https://github.com/CMU-CBML/HexGen_Hex2Spline. The hex mesh generation and volumetric spline construction algorithms are implemented in C++, utilizing the Eigen library [48] and Intel MKL [49] for matrix and vector operations and numerical linear algebra.

We have applied GCN, K-means, and two software packages to various models in a fully automated process. The results were computed on a PC equipped with a 3.1 GHz Intel Xeon w5-2445 CPU, 64 GB of RAM, a 16 GB GPU, and 32 GB of shared


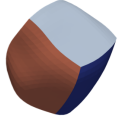
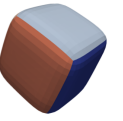
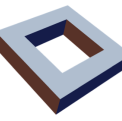

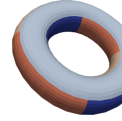
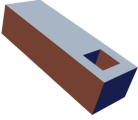
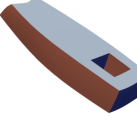
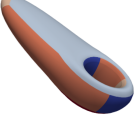
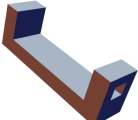

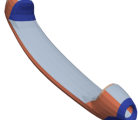
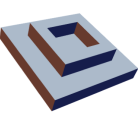
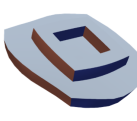
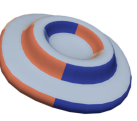

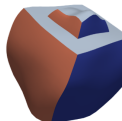
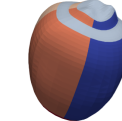

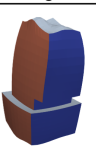
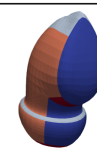

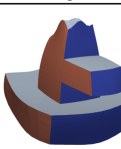
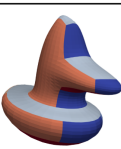
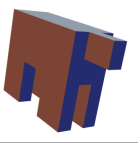
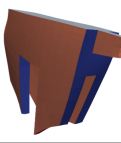
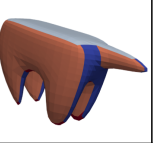
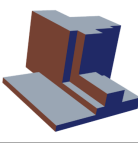
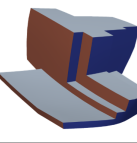
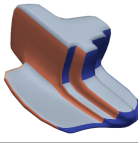
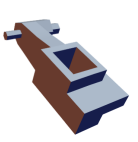

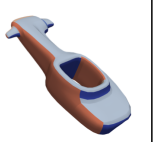
Type 1	Training Data with 1,728 Elements		Type 2	Training Data with 2,048 Elements	
					
Type 3	Training Data with 2,560 Elements		Type 4	Training Data with 1,536 Elements	
					
Type 5	Training Data with 3,840 Elements		Type 6	Training Data with 3,328 Elements	
					
Type 7	Training Data with 2,816 Elements		Type 8	Training Data with 3,328 Elements	
					
Type 9	Training Data with 1,984 Elements		Type 10	Training Data with 2,176 Elements	
					
Type 11	Training Data with 4,032 Elements				
					

Fig. 11: Visualization of the training dataset for the deep learning model. Polycube structures are shown on the left for each type, ordered by complexity, along with two randomly selected derivative geometries for each polycube type.

memory with an RTX 4080. The polycube structure is predicted using GCN-Polycube, while surface segmentation is based on K-means. If necessary, GCN-centroid is used to resolve segmentation issues that cannot be matched to the polycube structure when using only normal space in K-means. To address the zigzag problem, we employed Dijkstra's algorithm. Some initial triangular meshes have connectivity issues: if certain parts of the mesh are not connected, the Dijkstra algorithm may fail to find a smooth path from start to finish. Therefore, after identifying the polycube structure and encountering zigzag issues during segmentation, we refine the initial triangular mesh

Table 1: Probability distribution of predicted polycube structures for 16 CAD models.

Model	P1	P2	P3	P4	P5	P6	P7	P8	P9	P10	P11
ring (Fig. 1)	0.00	99.92	0.00	0.00	0.08	0.00	0.00	0.00	0.00	0.00	0.00
rod (Fig. 12)	0.00	0.00	100.00	0.00	0.00	0.00	0.00	0.00	0.00	0.00	0.00
arch mount (Fig. 12)	0.00	0.00	0.01	95.92	0.00	0.00	0.00	0.00	0.14	0.00	3.93
mount (Fig. 12)	0.00	0.12	0.04	0.00	99.82	0.01	0.00	0.00	0.00	0.00	0.01
CTP-cube (Fig. 13)	0.79	0.00	1.61	0.00	0.06	91.79	2.99	2.56	0.20	0.00	0.00
bust (Fig. 13)	0.14	0.00	0.00	0.00	0.00	5.26	89.60	0.00	5.00	0.00	0.00
duck (Fig. 13)	0.00	0.00	14.91	0.00	0.00	1.93	0.01	83.15	0.00	0.00	0.00
cow (Fig. 14)	0.00	0.00	0.00	0.00	0.00	0.00	0.00	0.00	100.00	0.00	0.00
fandisk (Fig. 14)	0.00	0.00	0.00	0.00	0.00	0.02	0.00	0.00	0.03	99.75	0.20
rockerarm (Fig. 14)	0.00	0.00	0.05	0.01	0.71	0.02	0.00	0.00	0.03	0.00	99.18
dice (Fig. 15)	65.13	0.00	0.00	0.00	0.00	34.60	0.27	0.00	0.00	0.00	0.00
cog (Fig. 15)	0.00	97.82	0.00	0.00	2.10	0.00	0.00	0.00	0.00	0.00	0.08
screw (Fig. 15)	0.00	0.00	0.03	0.00	0.00	99.75	0.02	0.20	0.00	0.00	0.00
knight (Fig. 15)	0.26	0.00	0.00	0.00	0.00	0.13	99.55	0.00	0.06	0.00	0.00
turtle (Fig. 15)	0.00	0.00	7.69	0.05	0.01	0.13	0.01	0.01	91.61	0.00	0.49
lion (Fig. 15)	0.00	0.00	2.56	0.00	0.00	0.08	0.00	0.00	97.36	0.00	0.00

to resolve these connectivity problems. The predicted polycube structure and surface segmentation are then used as inputs for HexGen and Hex2Spline, which generate high-quality all-hex meshes and splines. For selected ten models, we present the predicted polycube, surface segmentation, and the final all-hex mesh. The models include rod model (Fig. 1); ring, arch mount, and mount models (Fig. 12); cylinder-topped perforated cube (CTP-cube), bust, and duck models (Fig. 13); and cow, fandisk, and rockerarm models (Fig. 14). Table 2 provides statistics of all tested models. The quality of the all-hex meshes is assessed using the scaled Jacobian, the obtained meshes exhibit good quality (minimal Jacobian > 0.1).

After generating all-hex meshes, we tested these ten models for IGA using TH-spline3D. The result of the spline construction is C^0 -continuous around extraordinary points and edges, while maintaining C^2 -continuous in all other regions. Subsequently, Bézier elements are extracted for the IGA analysis. For each testing model, we use ANSYS-DYNA to perform eigenvalue analysis and show the first mode result (Figs. 1, 12, 13, and 14). The results indicate that our algorithm successfully produces valid volumetric spline structures for IGA applications in ANSYS-DYNA.

7 Conclusions and future work

In this paper, we present a novel approach called DL-Polycube, which integrates deep learning with the polycube method to automate the generation of high-quality hex meshes and volumetric splines. By incorporating deep learning, we significantly reduce the manual effort required for surface segmentation and polycube construction in our previously developed software packages [24] and improve correction procedures to address the issue where not every labeling permits a corresponding polycube, as mentioned in [11]. Since the labeling is automatically generated from the predicted polycube structure, these labelings naturally correspond to a polycube. Our approach leverages machine learning to automate the construction of polycube structures from

Table 2: Statistics of the tested models for hex mesh generation.

Model	Input triangle mesh (vertices elements)	Octree levels	Output hex mesh (vertices elements)	Worst Jacobian
ring (Fig. 12)	(1,536 3,072)	4	(22,592 20,480)	0.54
rod (Fig. 1)	(11,436 22,872)	3	(4,520 3,840)	0.28
arch mount (Fig. 12)	(38,592 77,184)	3	(5,832 4,608)	0.19
mount (Fig. 12)	(13,136 26,268)	3	(7,641 6,656)	0.16
CTP-cube (Fig. 13)	(1,122 2,240)	3	(9,317 8,448)	0.44
bust (Fig. 13)	(8,540 17,076)	3	(42,851 39,424)	0.20
duck (Fig. 13)	(12,217 24,372)	3	(7,547 6,528)	0.29
cow (Fig. 14)	(3,359 6,714)	3	(29,745 27,648)	0.61
fandisk (Fig. 14)	(25,894 51,784)	3	(33,001 30,720)	0.19
rockerarm (Fig. 14)	(69,936 139,872)	3	(68,136 64,000)	0.12

CAD geometries and the subsequent surface segmentation. The surfaces of the predicted polycube structures and the segmented CAD geometry maintain a one-to-one correspondence. This algorithm not only automates the conversion of CAD geometries into high-quality hex meshes but also reduces the learning curve for users, allowing them to quickly become familiar with in generating hex meshes and constructing volumetric splines. The robustness and efficiency of the DL-Polycube algorithm are demonstrated through several examples.

While the DL-Polycube algorithm represents a significant advancement in our early work on hex mesh generation and volumetric spline construction, there are several areas for future improvement. First, it is important to note that the variability of the design parameters and topologies within the dataset constrains the generalizability of the machine learning model. If the geometry model encounters design parameters and topologies outside its trained range, it may not predict an ideal polycube structure, leading to poor-quality hex mesh. Therefore, we plan to include a wider variety of design parameters and topologies in our dataset to cover more geometric configurations. A geometric library based on more polycubes can be established to facilitate this. Second, this paper focuses on genus-0 and genus-1 geometries. For high-genus geometries and complex genus-0 and genus-1 geometries, generative models can be employed to automatically separate them into multiple simpler genus-0 and genus-1 geometries, each simpler genus-0 or genus-1 geometry can then be processed using the methods described in this paper. This approach will enable the generation of hex meshes and the construction of splines for high-genus and complex geometries, which is an area of interest for us. Third, although our focus has been on hex meshes, extending the DL-Polycube algorithm to generate other types of meshes, such as hex-dominant meshes, could broaden its applicability.

In conclusion, the DL-Polycube algorithm represents a significant step forward in automating the hex mesh generation and volumetric spline construction. By addressing the future work, we aim to further enhance the capabilities and applicability of our approach, ultimately contributing to the advancement of hex mesh generation and IGA.

Acknowledgements. This project is supported by the National Natural Science Foundation of China (Grant No. 62302091), the Discipline Innovation Field Cultivation Project (Grant No. XKCX202308), and the Fundamental Research Funds for

the Central Universities (Grant No. 2232023D-24). H. Tong and Y. J. Zhang were supported in part by a Honda project.

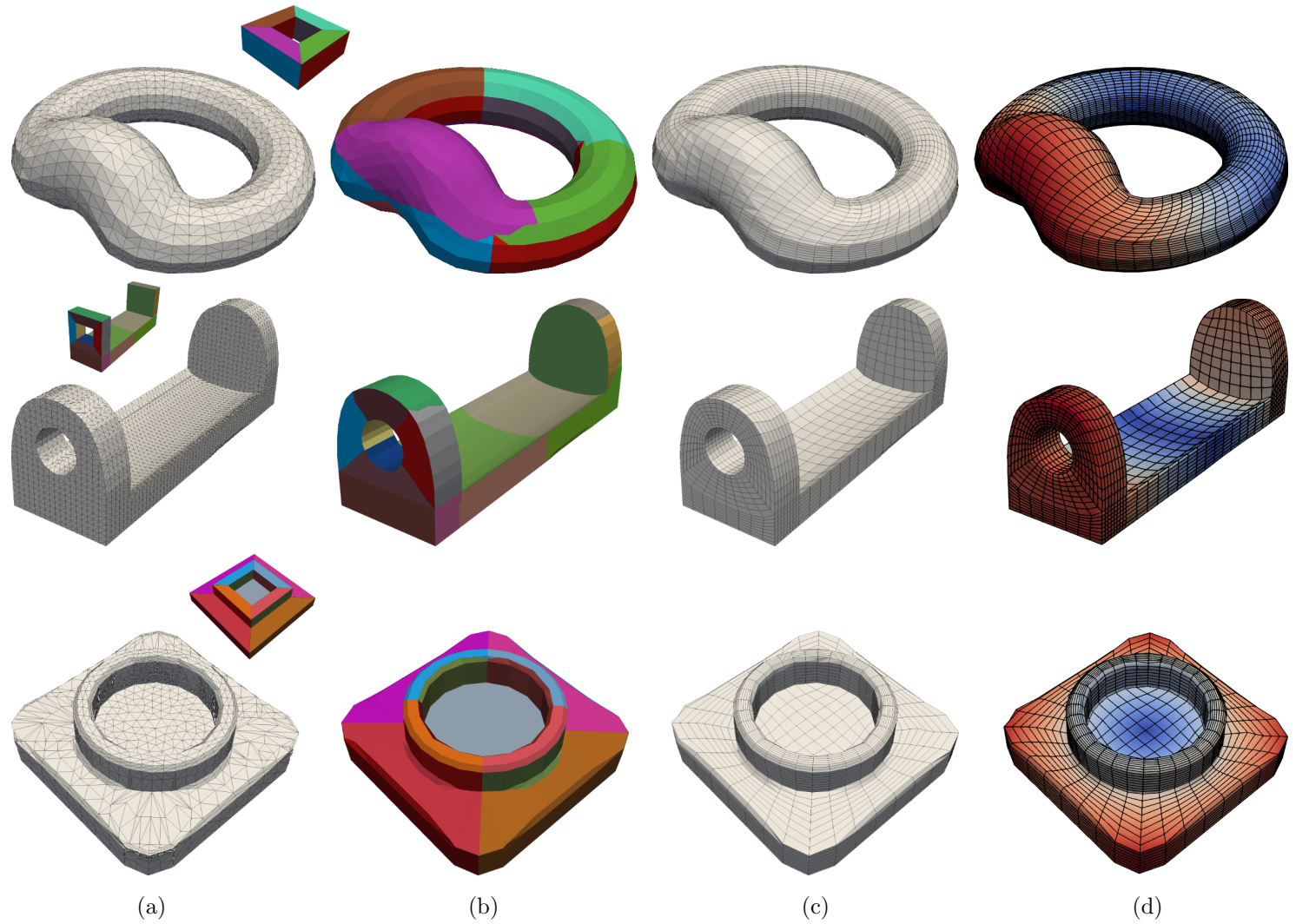


Fig. 12: Results of ring, arch mount, and mount models. (a) Surface triangle meshes with its predicted polycube structures; (b) segmentation results; (c) all-hex control meshes; (d) volumetric splines with IGA eigenvalue analysis in ANSYS-DYNA.

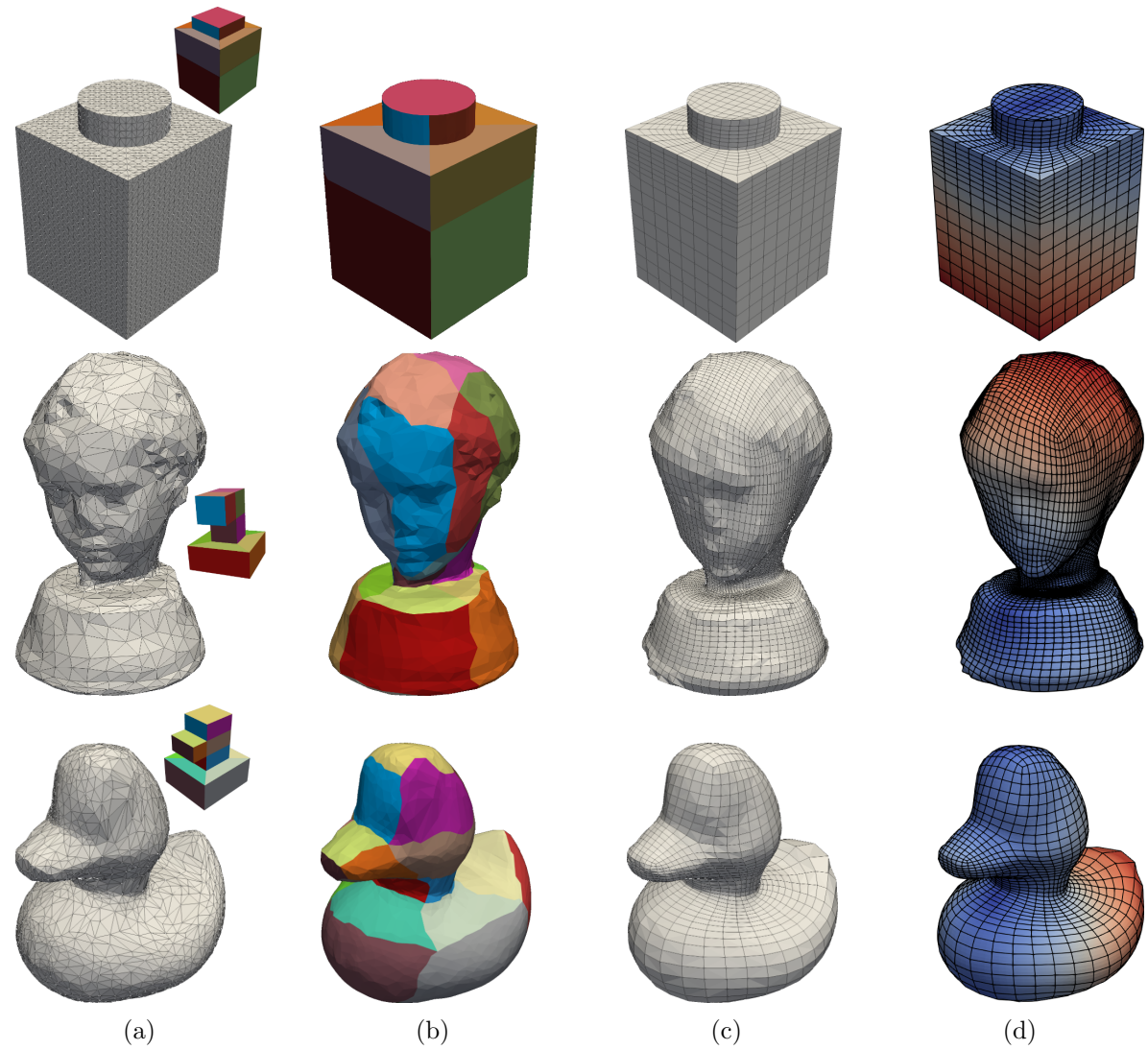


Fig. 13: Results of CTP-cube, bust, and duck models. (a) Surface triangle meshes with its predicted polycube structures; (b) segmentation results; (c) all-hex control meshes; (d) volumetric splines with IGA eigenvalue analysis in ANSYS-DYNA.

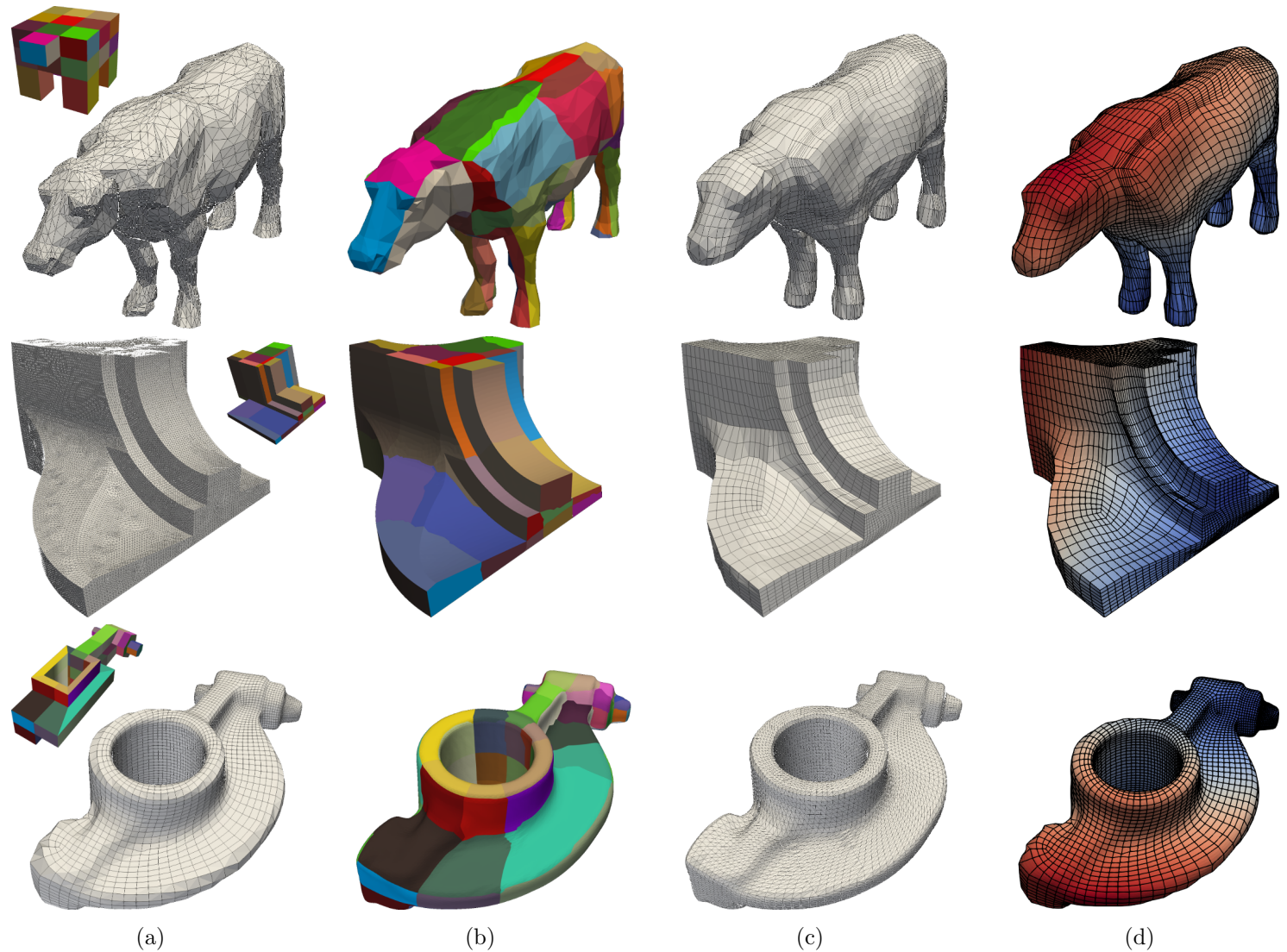


Fig. 14: Results of cow, fandisk and rockerarm models. (a) Surface triangle meshes with its predicted polycube structures; (b) segmentation results; (c) all-hex control meshes; (d) volumetric splines with IGA eigenvalue analysis in ANSYS-DYNA.

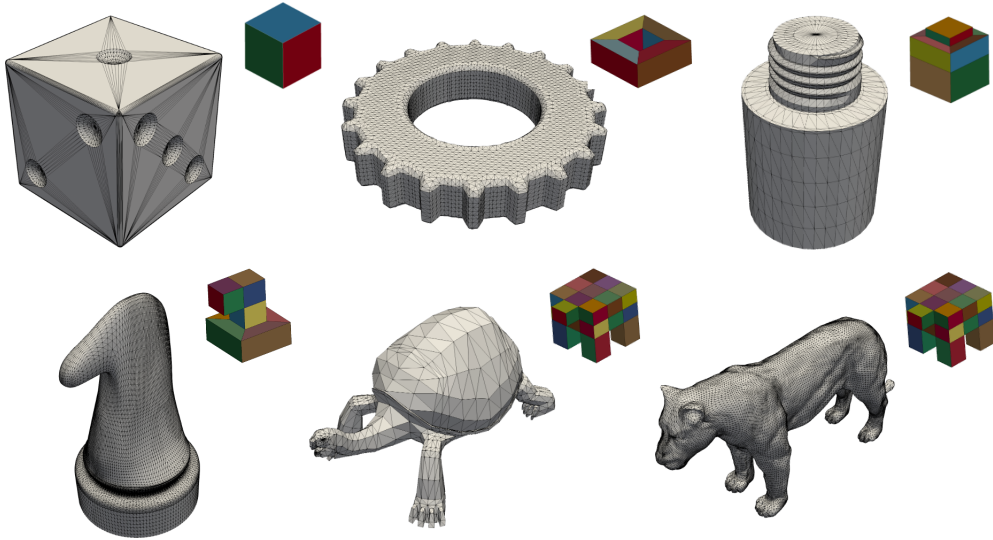


Fig. 15: Surface triangle meshes with predicted polycube structures for the additional six models.

References

- [1] Cottrell, J.A., Hughes, T.J., Bazilevs, Y.: *Isogeometric Analysis: Toward Integration of CAD and FEA*. John Wiley & Sons, (2009)
- [2] Hughes, T.J.R., Cottrell, J.A., Bazilevs, Y.: Isogeometric analysis: CAD, finite elements, NURBS, exact geometry, and mesh refinement. *Computer Methods in Applied Mechanics and Engineering* **194**, 4135–4195 (2005)
- [3] Sederberg, T.W., Zheng, J., Bakenov, A., Nasri, A.: T-splines and T-NURCCs. *ACM Transactions on Graphics* **22**, 477–484 (2003)
- [4] Li, X., Scott, M.A.: Analysis-suitable T-splines: Characterization, refineability, and approximation. *Mathematical Models and Methods in Applied Sciences* **24**(06), 1141–1164 (2014)
- [5] Wei, X., Li, X., Qian, K., Hughes, T.J.R., Zhang, Y.J., Casquero, H.: Analysis-suitable unstructured T-splines: Multiple extraordinary points per face. *Computer Methods in Applied Mechanics and Engineering* **391**, 114494 (2022)
- [6] Zuo, B., Huang, Z., Wang, Y., Wu, Z.: Isogeometric analysis for CSG models. *Computer Methods in Applied Mechanics and Engineering* **285**, 102–124 (2015)

- [7] Li, B., Li, X., Wang, K., Qin, H.: Generalized polycube trivariate splines. *Shape Modeling International Conference*, 261–265 (2010)
- [8] Zhang, Y., Wang, W., Hughes, T.J.R.: Solid T-spline construction from boundary representations for genus-zero geometry. *Computer Methods in Applied Mechanics and Engineering* **249-252**, 185–197 (2012)
- [9] Benzley, S.E., Perry, E., Merkley, K., Clark, B., Sjaardama, G.: A comparison of all hexagonal and all tetrahedral finite element meshes for elastic and elastoplastic analysis. *4th International Meshing Roundtable* **17**, 179–191 (1995)
- [10] Frâncu, M., Asgeirsson, A., Erleben, K., Rønnow, M.J.: Locking-proof tetrahedra. *ACM Transactions on Graphics* **40(2)**, 1–17 (2021)
- [11] Pietroni, N., Campen, M., Sheffer, A., Cherchi, G., Bommers, D., Gao, X., Scateni, R., Ledoux, F., Remacle, J., Livesu, M.: Hex-mesh generation and processing: A survey. *ACM Transactions on Graphics* **42(2)**, 1–44 (2023)
- [12] Zhang, Y.J.: *Geometric Modeling and Mesh Generation from Scanned Images*. Chapman and Hall/CRC, (2016)
- [13] Zhang, Y.J.: Challenges and advances in image-based geometric modeling and mesh generation. *Image-Based Geometric Modeling and Mesh Generation*, 1–10 (2013)
- [14] Eppstein, D.: Linear complexity hexahedral mesh generation. *Proceedings of the 12th Annual Symposium on Computational Geometry*, 58–67 (1996)
- [15] Zhang, Y.J., Bazilevs, Y., Goswami, S., Bajaj, C.L., Hughes, T.J.R.: Patient-specific vascular NURBS modeling for isogeometric analysis of blood flow. *Computer Methods in Applied Mechanics and Engineering* **196(29-30)**, 2943–2959 (2007)
- [16] Yu, Y., Zhang, Y.J., Takizawa, K., Tezduyar, T.E., Sasaki, T.: Anatomically realistic lumen motion representation in patient-specific space–time isogeometric flow analysis of coronary arteries with time-dependent medical-image data. *Computational Mechanics* **65(2)**, 395–404 (2020)
- [17] Qian, J., Zhang, Y.J.: Automatic unstructured all-hexahedral mesh generation from B-Reps for non-manifold CAD assemblies. *Engineering with Computers* **28(4)**, 345–359 (2012)
- [18] Schneiders, R.: A grid-based algorithm for the generation of hexahedral element meshes. *Engineering with Computers* **12(3-4)**, 168–177 (1996)
- [19] Qian, J., Zhang, Y., Wang, W., Lewis, A.C., Qidwai, M.A.S., Geltmacher, A.B.: Quality improvement of non-manifold hexahedral meshes for critical feature determination of microstructure materials. *International Journal for Numerical*

- Methods in Engineering **82**(11), 1406–1423 (2010)
- [20] Tarini, M., Hormann, K., Cignoni, P., Montani, C.: Polycube-maps. *ACM Transactions on Graphics* **23**(3), 853–860 (2004)
- [21] Wang, H., He, Y., Li, X., Gu, X., Qin, H.: Polycube splines. *Symposium on Solid and Physical Modeling*, 241–251 (2007)
- [22] Wang, W., Zhang, Y.J., Liu, L., Hughes, T.J.R.: Trivariate solid T-spline construction from boundary triangulations with arbitrary genus topology. *Computer Aided Design* **45**(2), 351–360 (2013)
- [23] Hu, K., Zhang, Y.J.: Centroidal Voronoi tessellation based polycube construction for adaptive all-hexahedral mesh generation. *Computer Methods in Applied Mechanics and Engineering* **305**, 405–421 (2016)
- [24] Yu, Y., Wei, X., Li, A., Liu, J., He, J., Zhang, Y.J.: HexGen and Hex2Spline: Polycube-based hexahedral mesh generation and spline modeling for isogeometric analysis applications in LS-DYNA. *Springer INdAM Series: Proceedings of INdAM Workshop “Geometric Challenges in Isogeometric Analysis.”* (2021)
- [25] Nieser, M., Reitebuch, U., Polthier, K.: Cubecover - parameterization of 3D volumes. *Computer Graphics Forum* **30**(5), 1397–1406 (2011)
- [26] Li, Y., Liu, Y., Xu, W., Wang, W., Guo, B.: All-hex meshing using singularity-restricted field. *ACM Transactions on Graphics* **31**(6), 1–11 (2012)
- [27] Lin, J., Jin, X., Fan, Z., Wang, C.: Automatic polycube-maps. *Advances in Geometric Modeling and Processing* **4975**, 3–16 (2008)
- [28] Hu, K., Zhang, Y., Liao, T.: Surface segmentation for polycube construction based on generalized centroidal Voronoi tessellation. *Computer Methods in Applied Mechanics and Engineering* **316**, 280–296 (2017)
- [29] Guo, H., Liu, X., Yan, D., Liu, Y.: Cut-enhanced polycube-maps for feature-aware all-hex meshing. *ACM Transactions on Graphics* **39**(4), 1–14 (2020)
- [30] Li, B., Li, X., Wang, K., Qin, H.: Surface mesh to volumetric spline conversion with generalized polycubes. *IEEE Transactions on Visualization and Computer Graphics* **99**, 1–14 (2013)
- [31] Wei, X., Zhang, Y., Hughes, T.J.R.: Truncated hierarchical tricubic C^0 spline construction on unstructured hexahedral meshes for isogeometric analysis applications. *Computers and Mathematics with Applications* **74**(9), 2203–2220 (2017)
- [32] Xu, G., Li, B., Shu, L., Chen, L., Xu, J., Khajah, T.: Efficient r-adaptive isogeometric analysis with Winslow’s mapping and monitor function approach. *Journal of Computational and Applied Mathematics* **351**, 186–197 (2019)

- [33] Gregson, J., Sheffer, A., Zhang, E.: All-Hex mesh generation via volumetric polycube deformation. *Computer Graphics Forum* **30**(5), 1407–1416 (2011)
- [34] Mandad, M., Chen, R., Bommers, D., Campen, M.: Intrinsic mixed-integer polycubes for hexahedral meshing. *Computer Aided Geometric Design* **94**, 102078 (2022)
- [35] Livesu, M., Vining, N., Sheffer, A., Gregson, J., Scateni, R.: Polycut: Monotone graph-cuts for polycube base-complex construction. *ACM Transactions on Graphics* **32**(6), 1–12 (2013)
- [36] Eppstein, D., Mumford, E.: Steinitz theorems for orthogonal polyhedra. *Proceedings of the 26th Annual Symposium on Computational Geometry*, 429–438 (2010)
- [37] Floater, M.S.: Parametrization and smooth approximation of surface triangulations. *Computer Aided Geometric Design* **14**(3), 231–250 (1997)
- [38] Zhang, Y., Bajaj, C.L., Xu, G.: Surface smoothing and quality improvement of quadrilateral/hexahedral meshes with geometric flow. *Communications in Numerical Methods in Engineering* **25**(1), 1–18 (2009)
- [39] Tong, H., Halilaj, E., Zhang, Y.J.: HybridOctree_hex: Hybrid octree-based adaptive all-hexahedral mesh generation with Jacobian control. *Journal of Computational Science* **78**, 102278 (2024)
- [40] Botsch, M.: *Polygon Mesh Processing*. A K Peters, (2010)
- [41] Sederberg, T.W., Parry, S.R.: Free-form deformation of solid geometric models. *Proceedings of the 13th Annual Conference on Computer Graphics and Interactive Techniques*, 151–160 (1986)
- [42] Liu, L., Zhang, Y.J., Liu, Y., Wang, W.: Feature-preserving T-mesh construction using skeleton-based polycubes. *Computer Aided Design* **58**, 162–172 (2015)
- [43] Zhang, Y., Wang, W., Hughes, T.J.R.: Conformal solid T-spline construction from boundary T-spline representations. *Computational Mechanics* **51**(6), 1051–1059 (2013)
- [44] Kipf, T.N., Welling, M.: Semi-supervised classification with graph convolutional networks. *arXiv:1609.02907* (2016)
- [45] Eck, M., DeRose, T., Duchamp, T., Hoppe, H., Lounsbery, M., Stuetzle, W.: Multiresolution analysis of arbitrary meshes. *Proceedings of the 22nd Annual Conference on Computer Graphics and Interactive Techniques*, 173–182 (1995)
- [46] Zhang, Y., Bajaj, C.: Adaptive and quality quadrilateral/hexahedral meshing from volumetric data. *Computer Methods in Applied Mechanics and Engineering*

195(9-12), 942–960 (2006)

- [47] Fey, M., Lenssen, J.E.: Fast graph representation learning with PyTorch Geometric. arXiv:1903.02428 (2019)
- [48] Guennebaud, G., Jacob, B.: Eigen v3. <http://eigen.tuxfamily.org> (2010)
- [49] Intel: Math kernel library. <https://software.intel.com/en-us/intel-mkl>